Plasma Physics Reports, Vol. 23, No. 11 1997, pp. 911–923. Translated from Fizika Plazmy, Vol. 23, No. 11, 1997, pp. 988–1001.

MAGNETIC CONFINEMENT SYSTEMS

Production of a Hot Initial Plasma in the End Cell of the Ambal-M Device

T. D. Akhmetov, V. S. Belkin, E. D. Bender, V. I. Davydenko, G. I. Dimov, A. N. Dranichnikov, E. A. Gilev, V. G. Igoshin, A. A. Kabantsev, Yu. V. Kovalenko, M. B. Persov, V. B. Reva, V. Ya. Savkin, V. G. Sokolov, and S. Yu. Taskaev

Budker Institute of Nuclear Physics, Siberian Division, Russian Academy of Sciences, Novosibirsk, 630090 Russia

Received November 25, 1996; in final form, March 18, 1997

Abstract—Methods of production and properties of a hot initial plasma in the end cell of the Ambal-M fully axisymmetric tandem mirror device are experimentally studied. Plasma produced in the end mirror device (end cell) has an electron temperature of ~ 50 eV, an ion energy of ~ 200 eV, and an average density of 6×10^{12} cm^{-3}. A plasma jet generated by the annular arc gas-discharge source and located behind the magnetic mirror is used to produce the initial plasma. Electrostatic fluctuations with a broad spectrum occurring in the plasma jet cause stochastic ion heating and subsequent heating of electrons. The most decisive factor in creating the hot initial plasma in the end cell is the thermal insulation, which suppresses the electron heat exchange between the end cell and the transport region. The studies performed show that, at both the plasma periphery and the axis, electron thermal insulation is provided by a plasma potential that has a minimum at the input mirror, whereas, in the intermediate region around the axis, the heat transport from the end mirror device is almost absent because of the high average velocity of the electron flow in the input mirror of the device. It is discovered that a 1 kA longitudinal flow of transit electrons provides effective electron heating in the end mirror device. Low-frequency plasma turbulence spectra are studied, the diffusion coefficients related to the electrostatic and magnetic transverse transport are determined, and the longitudinal losses of particles and energy are measured. The initial plasma produced is MHD stable in both the filling and decay stages. It is shown that the accumulation rate of trapped fast protons during the pulse injection of powerful beams of fast neutrals is sufficiently high.

INTRODUCTION

AMBAL-M, which is a tandem mirror device (MD) proposed by the Budker Institute of Nuclear Physics, Siberian Division, Russian Academy of Sciences [1–4], is an installation for experimental studies of confinement of high-temperature plasma in a nuclear fusion reactor. The magnetic field in the Ambal-M tandem MD is fully axisymmetric, and therefore, there are no neoclassical plasma losses in this system. At the present time, experiments are being carried out with the end cell of the device, which includes a barrier MD and a semi-cusp; the goal of the experiments is to produce a dense, long-lived, high-temperature plasma.

We used several methods for providing MHD plasma stability in the axisymmetric end cell. A semi-cusp connected to it can provide MHD stability when hot ions are produced there by using the injection of beams of fast hydrogen atoms or the ion cyclotron resonance (ICR) heating. However, the main planned method for obtaining and studying the MHD stabilization of high-pressure plasma with an anisotropic distribution of high-temperature particles is to use the conducting shell. In the end barrier MD, it is possible to produce a high-pressure hot-electron gas by using two-frequency electron cyclotron resonance (ECR) heating with a power up to 0.7 MW, as well as a dense gas of hot ions by injecting beams of fast deuterium atoms with a power up to several megawatts. MHD plasma stability in the transient regimes can be provided by using a semi-cusp or by "freezing" the magnetic field lines into the ends with the help of annular gas-discharge cells placed at the plasma collectors.

In order to perform these experiments, it is very important to have an initial target plasma with a high electron temperature. For a moderate density of the target plasma, the trapping of fast ions from the injected beam (which consists of fast atoms) is proportional to the target plasma density. The main process, which determines the behavior of the trapped fast ions, is deceleration by electrons with the energy loss rate $\frac{dE_i}{dt} = -\frac{E_i}{\tau_{ie}}$, where $\tau_{ie} \approx \frac{3MT_e^{3/2}}{8\sqrt{2\pi}e^4\lambda\sqrt{mn}}$. Therefore, to a first approximation, the equilibrium density of trapped ions $n_i \propto n\tau_{ie}$ is independent of the target plasma density and depends on the electron temperature as $T_e^{3/2}$. In order to obtain the equilibrium density of the trapped ions, the target plasma must be confined for several deceleration times. Another factor affecting the confinement time of trapped ions is the charge-exchange loss; in order to decrease this loss, the time required for obtaining the equilibrium density of trapped ions must be decreased.

1063-780X/97/2311-0911$10.00 © 1997 МАИК Наука/Interperiodica Publishing

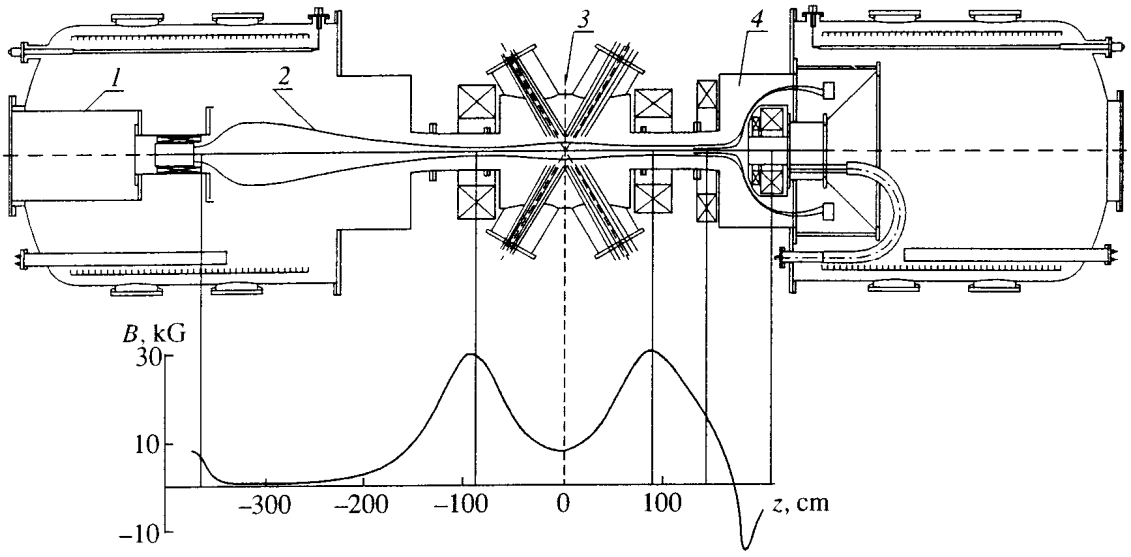

Fig. 1. Diagram of the end cell experiment: (*1*) plasma source; (*2*) transport region; (*3*) MD; and (*4*) semi-cusp.

and, accordingly, the density of the target plasma must be increased.

A high electron temperature in the target plasma is also necessary for producing the dense hot-electron gas by the ECR heating at the second harmonic, since both the absorption of the microwave power and the rate of growth of the fast electron energy increase with an increase in the electron temperature. In [5], the formation of the hot-electron gas in the end MD of the Ambal-M is discussed in detail; it is shown that, for the efficient absorption of microwave power, it is necessary to have a target plasma with a density up to 10^{13} cm^{-3} and an electron temperature no less than 50 eV.

In order to produce the target plasma in the end cell of the Ambal-M, we used a gas-discharge annular plasma source [6] placed behind the mirror. An important feature of the plasma jet generated by this source is the presence of the longitudinal currents and transverse electric field inside the jet. This electric field causes the onset of the Kelvin–Helmholtz instability, resulting in a wide spectrum of electrostatic oscillations with subsequent stochastic anisotropic ion, and then electron heating. Due to anisotropy of the ion distribution function (the transverse energy is higher than the longitudinal energy), a considerable fraction of the ion flow can be reflected from the mirror; as a result, the local density decreases, and the thermal barrier arises. Such conditions are typical of the Ambal- Yu MD with the quadrupole magnetic field [7], when the annular gas-discharge source is used. A thermal barrier in the mirror makes it possible to obtain plasma with an electron temperature ≥50 eV and ion energy of 1 keV. The use of the annular gas-discharge source in the Ambal-M end cell also seems to be a promising method for producing the hot initial plasma. A plasma with an electron temperature of 50 eV, an ion energy of 200 eV, and a density of 6×10^{12} cm^{-3} was produced in the end cell in experiment [8]. Due to the axial symmetry of the end MD of the Ambal-M, its input size is larger than the cross section of the mirror of the quadrupole MD, and this allows us to study the thermal insulation at different radii. This paper is aimed at the investigation of parameters and mechanisms of production of the hot initial plasma in the end cell of the Ambal-M axisymmetric tandem MD.

EXPERIMENTAL SETUP

The end cell of the Ambal-M and the experimental program for this device are described in detail in [4, 9]. Figure 1 shows the schematic of production of the initial plasma in the end cell. The annular gas-discharge source is placed in the shell of the plasma collector inside the pulse solenoid, which provides the matching conditions for the initial diameter of the plasma jet and the diameter of end-cell plasma. The duration of the pulse of the source discharge current is 1.8 ms. The plasma from the source passes through the transport region and enters the end MD. The distance between mirrors of the end MD is 1.7 m and the mirror ratio is $R = 4$. A semi-cusp is connected to the output of the MD; the field in the cusp is created by a coil located inside the vacuum chamber.

Figure 2 shows diagnostics used for studying the behavior and parameters of the initial plasma. Langmuir probes placed in eight cross sections can be moved along the radius and measure the float potential and the probe characteristics. In addition, sets of Langmuir probes are located in the azimuthal direction in the MD. The radial and azimuthal structure of the plasma

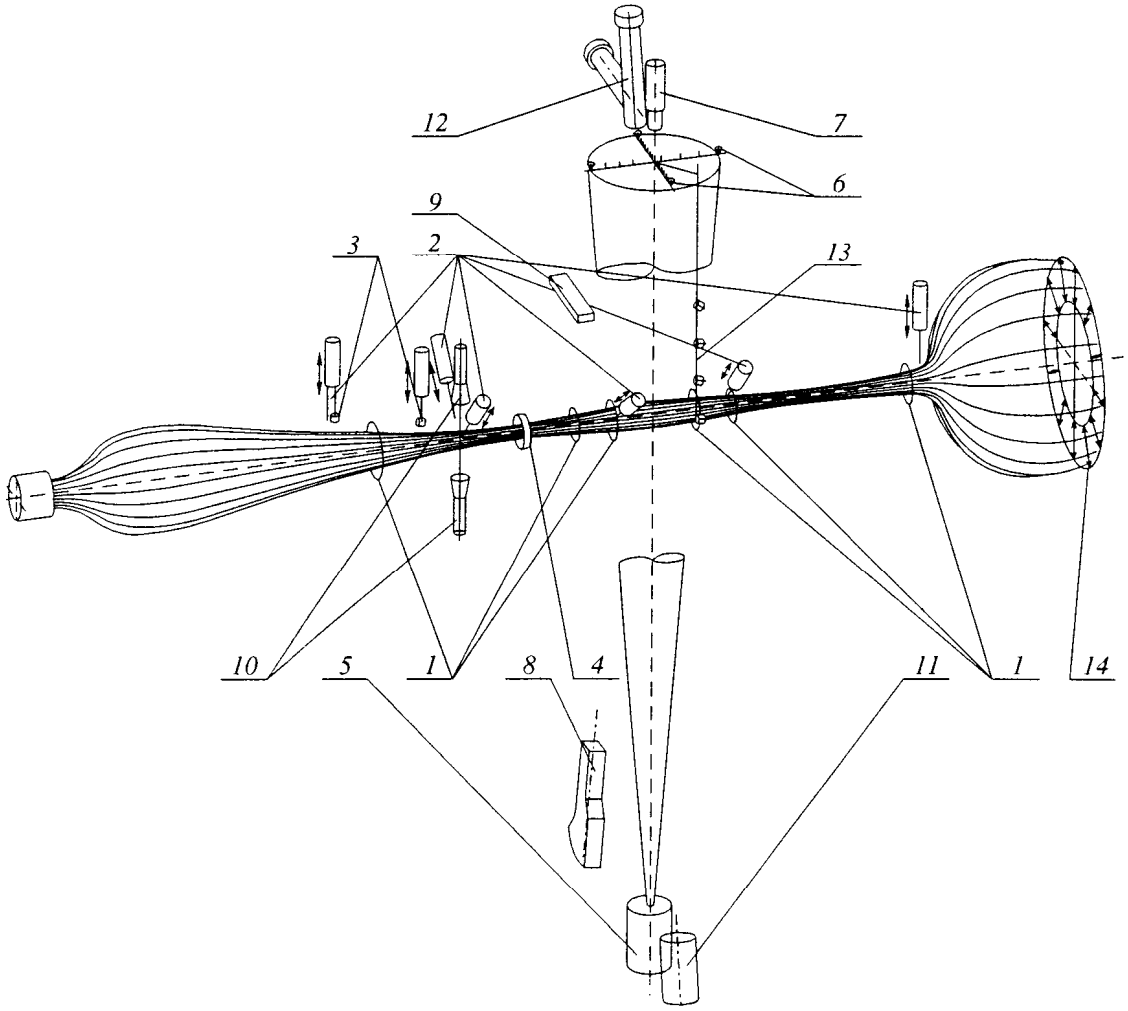

Fig. 2. Diagnostics: (*1*) diamagnetic loops; (*2*) Langmuir probes; (*3*) magnetic probes; (*4*) Rogowski loop; (*5*) diagnostic injector of fast neutrals; (*6*) multichord probing detectors; (*7*) time-of-flight analyzer; (*8*) 5-channel charge exchange analyzer; (*9*) optical spectrometer; (*10*) MW interferometer. (*11*) X-ray spectrometer; (*12*) detector of H_α and H_β line radiation; (*13*) fast operating vacuum gauges; and (*14*) end plasma-flow detectors.

flow leaving the semi-cusp is measured by detectors in the end plasma collector and a movable detector located near the axis behind the semi-cusp coil. Plasma energy is determined by diamagnetic loops. The longitudinal plasma current is measured by the Rogowski loop placed in front of the input mirror, and its radial profile is determined from measurements of the azimuthal magnetic field by using a movable coil 1 cm in diameter enclosed by an insulating shell made of boron nitride. Some contactless diagnostics are used to measure plasma parameters in the equatorial plane of the end MD: the probing of plasma by fast hydrogen atom beams along the various chords [10], measurement of the electron temperature by attenuation of the argon atom beam, H_α emission measurements along various chords, measurement of the visible emission by monochromator, and X-ray spectrometry. A set of fast vacuum gauges of the magnetron type [11] is used to measure pressure in the MD.

EXPERIMENTAL RESULTS

Parameters of the Mirror Device Plasma

The measurements show that plasma produced in the MD is indeed hot. Figure. 3 shows the time dependence of the ion temperature measured by Doppler broadening of the H_α line. It is seen that temperature attains a value of T_i = 200 eV toward the end of the plasma source discharge. The electron temperature measured by probes is in the range 40–50 eV. X-ray spectrometry gives an electron temperature of 50 eV. Figure 4 presents the radial profile of the plasma density in the center of the MD (z = 0); the profile is obtained from Abel inversion of multichord measurements of attenuation of an 8-keV hydrogen atom diag-

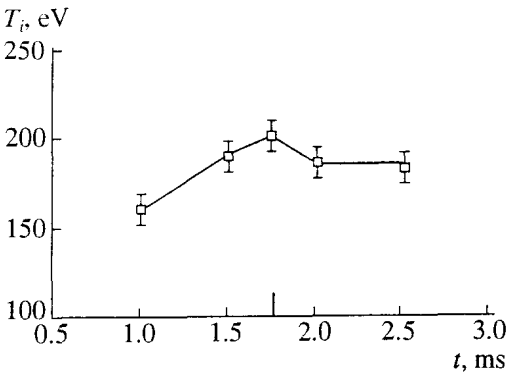

Fig. 3. Ion temperature in the center of the MD as a function of time. Termination of the discharge in the plasma source is marked by the line segment.

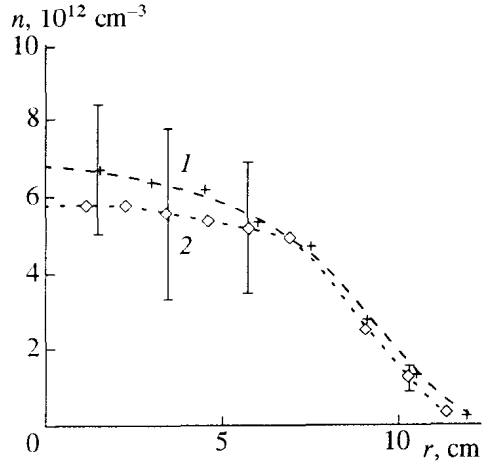

Fig. 4. Radial profiles of the plasma density in the central plane (*1*) of the MD and in the plane $z = 25$ cm (*2*).

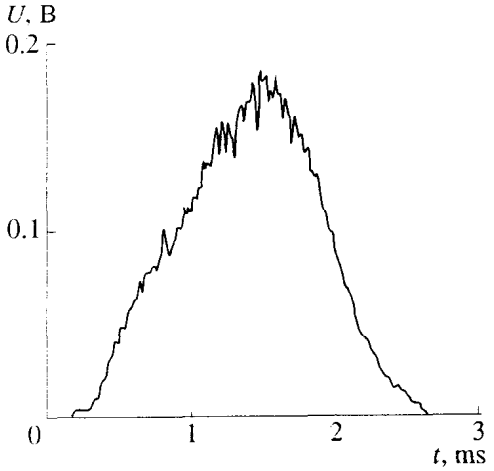

Fig. 5. Time dependence of the diamagnetic signal from the initial plasma in the MD ($z = 25$ cm).

nostic beam. The radial profile of the plasma density measured by the probe at the distance $z = -25$ cm from the center of the MD is also shown in Fig. 4. The time dependence of the diamagnetic signal measured at the distance $z = 25$ cm is shown in Fig. 5. The obtained value of the diamagnetic energy per unit length $n(T_i + T_e)S \approx 1.5 \times 10^{17}$ eV/cm agrees with the data from other measurements.

Plasma Parameters in the Transport Region and in the Mirror Device

In order to understand the cause of plasma thermal insulation in the MD, a series of Langmuir probe measurements were carried out at several cross sections in the transport region and in the MD. The probe floating potential averaged over several oscillation periods and the ion saturation current were reliably determined from these measurements. The interpretation of the electron-current part of the probe characteristics and determination of the electron temperature, average electron energy, and plasma potential from the probe data is rather difficult. This is because of the nonclassical character of the characteristics, which seems to be due to both the non-Maxwellian electron distribution function and considerable electron energy causing appreciable secondary electron emission. The processing of the probe characteristics has shown that, under the given conditions, the difference between the plasma potential and the probe floating potential is of order $2T_e/e$. The longitudinal distributions of electron temperature in the transport region and in the MD are shown in Fig. 6. Figure 7 presents the characteristic distributions of the plasma potential along four magnetic field lines from the plasma source to the output mirror of the MD. The potential is determined from the measured values of the floating potential and electron temperature. Figure 8 shows the plasma density profiles along the axis and along the magnetic field line originating at the radius equal to the half-radius of the gas-discharge channel of the plasma source. It is seen that there is a minimum of the plasma density in the input mirror region, whereas at the axis, at the plasma periphery, and at the magnetic field lines originating at the source discharge channel a well-defined potential minimum is created in the input mirror. Near the input mirror, at the magnetic field lines close to the axis, the plasma potential decreases despite the decrease in the plasma density. In the MD, there is a maximum of the potential related to the elevated plasma density.

Longitudinal Electron Current in the Initial Plasma

An important factor governing the electron behavior in the end cell is the 1.6–1.0 kA electron current flowing along the plasma jet during the plasma source pulse. A typical time dependence of the azimuthal magnetic field signal is shown in Fig. 9. Figure 10 presents the radial profiles of the current density obtained by

processing these signals (the radial coordinate is normalized by a factor incorporating squeezing or extention of magnetic field lines with respect to the output cross section of the plasma source). It is seen that, close to the outlet of the plasma source, the electron current profile is hollow; however, closer to the input mirror, the current fills all the plasma jet cross section. Maximum electron current flowing toward the plasma collector is 1.6 kA in the transport region and 1.0 kA at the entrance to the semi-cusp. At the plasma periphery, there is a reverse current; the typical value of this current is 0.4 kA.

Studies of the Initial Plasma Oscillations

In the end-cell plasma, there is a turbulence with a wide spectrum of oscillations. The most intense turbulence is due to the Kelvin–Helmholtz instability, which is driven during the plasma beam production by the annular gas-discharge plasma source. This turbulence was studied in [12]. Figure 11 shows the characteristic radial profile of the probe floating potential measured in the transport region during the current pulse of the plasma source. This instability is caused by the radial inhomogeneity of the electric field with a magnitude up to 100 V/cm, which is directed toward the axis. It is seen from the time dependences of the plasma floating potential (Fig. 12) that, during the source operation, oscillations with an amplitude up to 200 V are present in the plasma. Averaged potential varies during the pulse from –400 V at the beginning of the discharge to –100 V at the end, which is related to a decrease in the discharge voltage in the plasma source. Figure 13 shows the spectrum of oscillations of the probe floating potential, which corresponds to the 200 μs time interval and is taken at 1000 μs after the beginning of the pulse of the plasma source current. In the low-frequency part of the spectrum, there are maximums at frequencies corresponding to the harmonics of the fundamental frequency, which result from the azimuthal drift of the corresponding azimuthal harmonics. The fundamental frequency decreases during the pulse from 24–26 kHz at the beginning of the discharge to 10–12 kHz at the end, which is related to the above-mentioned decrease in the discharge voltage. The high-frequency part of the fluctuation spectrum has no distinct maximums and monotonically decreases as frequency increases. The measurements of the potential difference between the probes placed at 1 cm distance in the azimuthal direction give the amplitude of oscillations of the azimuthal electric field $E \approx 100$ V/cm.

In addition to the electrostatic fluctuations, the magnetic field fluctuations are also present in the initial plasma during the plasma source operation. These fluctuations are most substantial in the transport region, where the magnetic field is lower. Figures 14 and 15 show the radial dependence of the fluctuation amplitude in the transport region and the fluctuation spectrum, respectively.

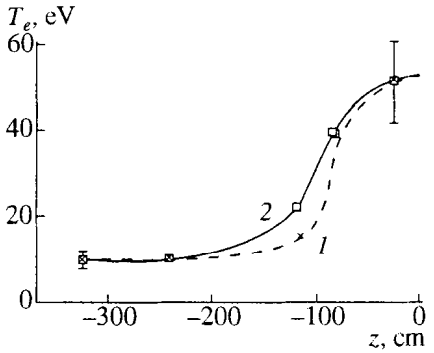

Fig. 6. Longitudinal distributions of the electron temperature: (*1*) along the magnetic field line originating in the gas discharge channel of the plasma source and (*2*) along the magnetic field line passing through the radius equal to the half-radius of the gas discharge channel.

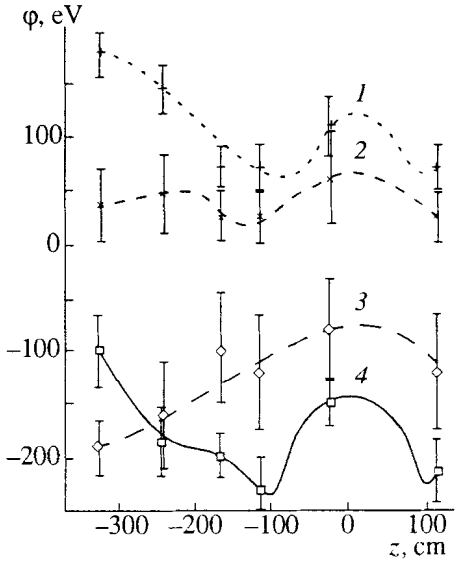

Fig. 7. Longitudinal profiles of the plasma potential in the transport region and in the MD: (*1*) at the periphery, (*2*) along the magnetic field line originating in the gas discharge channel of the plasma source, (*3*) along the magnetic field line passing through the radius equal to the half-radius of the gas discharge channel, and (*4*) along the axis.

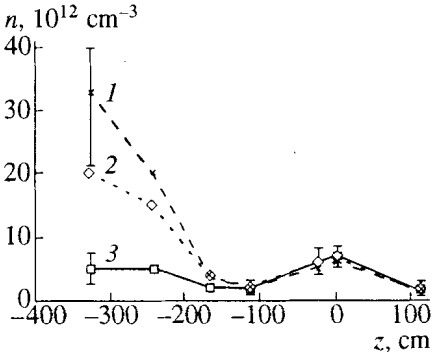

Fig. 8. Longitudinal profiles of the plasma density: (*1*) along the magnetic field line originating in the gas discharge channel of the plasma source, (*2*) along the magnetic field line passing through the radius equal to the half-radius of the gas discharge channel, and (*3*) along the axis.

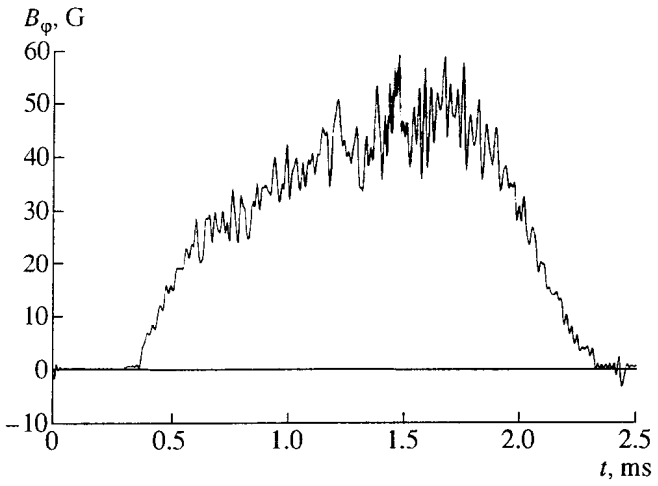

Fig. 9. Time dependence of the signal from the magnetic probe measuring the azimuthal magnetic field.

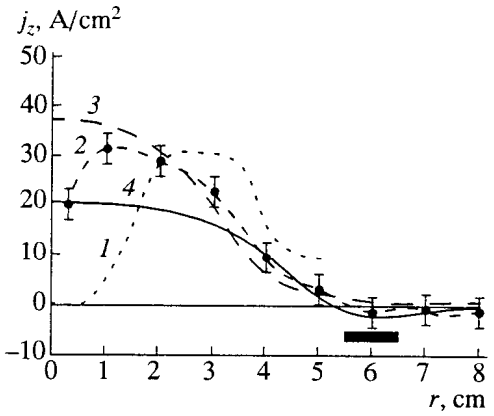

Fig. 10. Radial profiles of the longitudinal current density (the radial coordinate is normalized by a factor incorporating squeezing or extension of magnetic field lines with respect to the output cross section of the plasma source) at (*1*) $z = -243$ cm, (*2*) $z = -168$ cm, (*3*) $z = 25$ cm, and (*4*) $z = 168$ cm. Position of the gas-discharge channel is marked with the bold line segment.

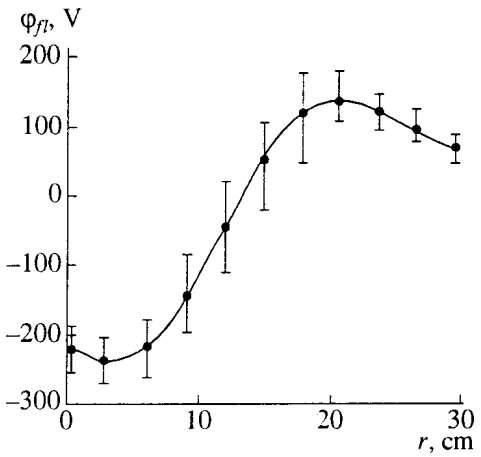

Fig. 11. Radial profile of the probe floating potential in the transport region ($z = -243$ cm).

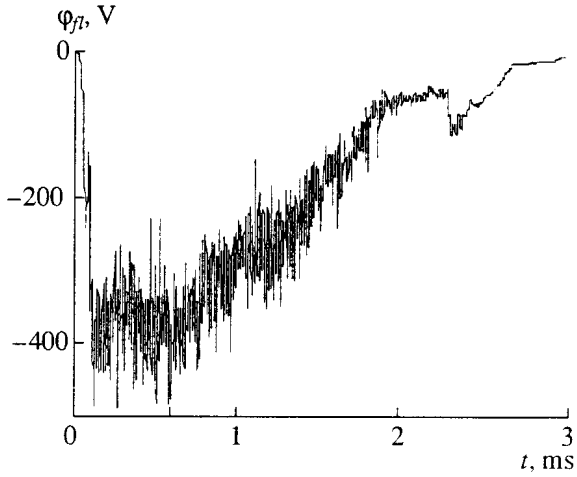

Fig. 12. Time dependence of the probe floating potential ($z = -115$ cm).

Plasma Diffusion

Excitation of the plasma oscillations results in increased diffusion. The value of the diffusion coefficient can be determined from the change in the density profiles in different cross sections. In particular, Fig. 16 presents the radial plasma density profile in the transport region in the initial stage of filling the central cell. The diffusion coefficient estimated from the rate of change of the radial plasma density profile is $\sim 2 \times 10^5$ cm^2/s; this value agrees with the diffusion coefficient obtained previously in studies of transport of the annular plasma jet generated by a similar plasma source in the axisymmetric magnetic field [12].

From correlations between density fluctuations and fluctuations of the azimuthal electric and radial magnetic fields, it is possible to determine the local transport velocities and diffusion coefficients related to the electrostatic and magnetic transport mechanisms [13]. The transport processes resulting from the electrostatic fluctuations were studied with the help of a double probe measuring the potential and the ion saturation current. The azimuthal electric field was determined from the angular harmonic spectrum. The degree of coherence of fluctuations of the plasma density and azimuthal electric field is shown in Fig. 17. The local diffusion coefficient related to the electrostatic transport is determined from the correlated part of the radial flow and the density gradient; it is $\sim 2 \times 10^5$ cm/s, which corresponds to the value of the integrated diffusion coefficient.

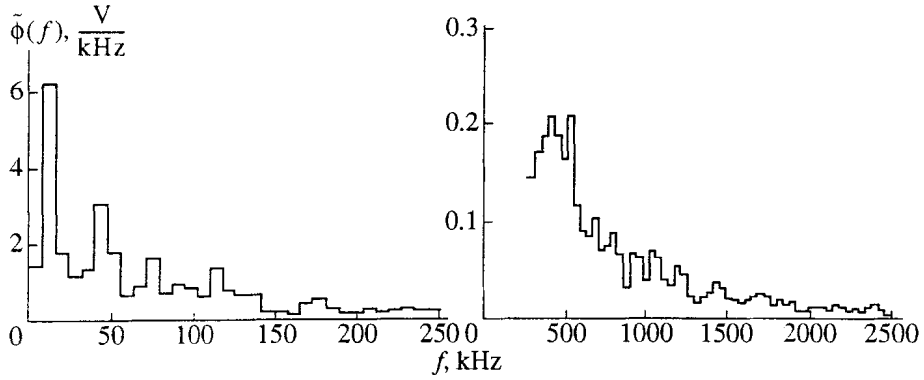

Fig. 13. Spectrum of the electrostatic fluctuations in the input mirror.

In order to study the transport processes caused by the magnetic field fluctuations, we used a detector, in which a small-size coil measured fluctuations of the radial magnetic field and a Langmuir probe measured the plasma density. For determining the radial particle flux related to these fluctuations, we used the Fourier expansion in terms of frequency $\Gamma_r(\omega) \propto n^*(\omega)B_r(\omega)\cos(\varphi(\omega))$, where $\varphi(\omega)$ is the phase shift between oscillations of density and radial magnetic field. The fluctuations of radial magnetic field and density turned out to be correlated only in some frequency interval near the fundamental frequency (Fig. 18). The diffusion coefficient related to the radial magnetic field fluctuations is $\sim 10^4$ cm^2/s, which is an order of magnitude less than the electrostatic diffusion coefficient.

During plasma decay, the level of oscillations and the diffusion coefficient decrease. In order to estimate the integrated diffusion coefficient at this stage, we measured the radial profile of the ion saturation current to the Langmuir probe in the MD, as well as the profile of the ion flow to the end plasma collector. The profile of the ion flow turns out to be trapezoid-like (Fig. 4) and conserves its shape over all the decay stage. For the cylindrical geometry, the analytical solution to the diffusion equation can be written in the form of expansion in Bessel functions in which each harmonic has its own decay time. The profile obtained is different from $J_0(2.4R/R_0)$, where J_0 is the zeroth Bessel function, R_0 is the radius of the diaphragm closest to the plasma; this is evidence for the presence of higher harmonics with smaller decay time. As the numerical simulations show, the conservation of the radial profile of the flow to an accuracy of 5–10% means that the diffusion coefficient in the decay stage does not exceed the value of 10^3 cm^2/s.

Longitudinal and Transverse Losses

The output ion flow was measured by a set of detectors located at the semi-cusp plasma collector and by the probes located behind the aperture of the semi-cusp coil. Measurements were made in the ion-current saturation regime. Fig. 19 shows the measured flow profiles. As it can be seen from the profile of the density of the current to the annular plasma collector, a part of the flow penetrates into the region outside of the magnetic field separatrix. The characteristic penetration depth corresponds to the nonadiabatic region of the semi-cusp, which was calculated for 200 eV ion energy [14]. The profile of the ion flow through the axial mirror of

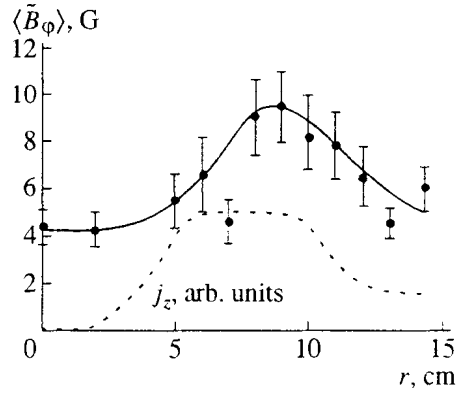

Fig. 14. Amplitude of fluctuations of the azimuthal magnetic field in the transport region as a function of radius.

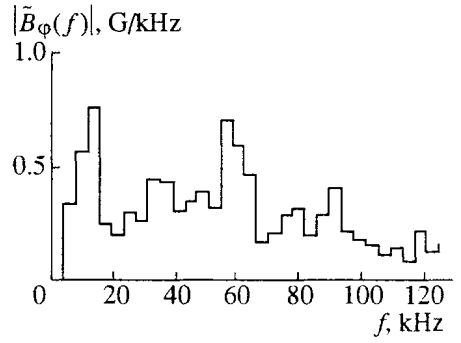

Fig. 15. Spectrum of fluctuations of the azimuthal magnetic field in the transport region.

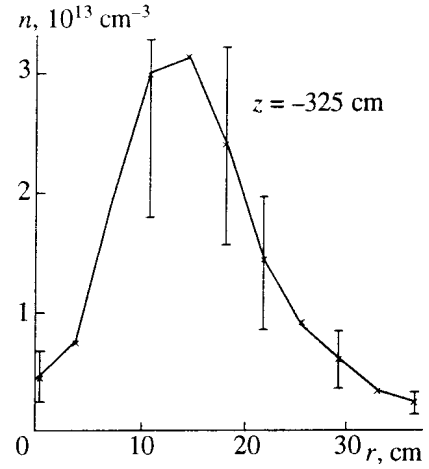

Fig. 16. Radial profile of the plasma density in the transport region at $z = -325$ cm.

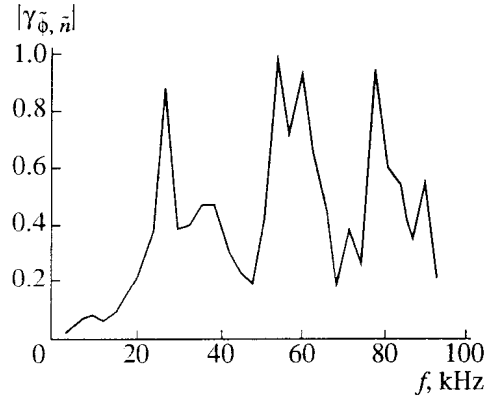

Fig. 17. Coherence spectrum of density fluctuations and fluctuations of the azimuthal magnetic field in the input mirror.

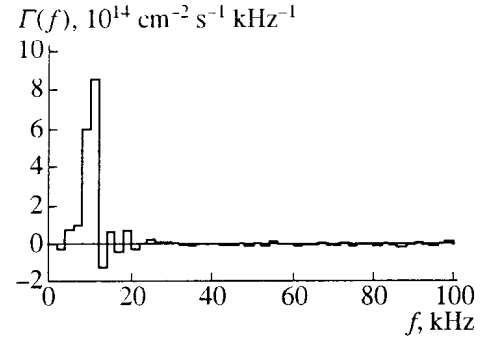

Fig. 18. Spectrum of fluctuations of the particle flow caused by magnetic fluctuations in the transport region.

the semi-cusp, which is approximated by a Gaussian, also corresponds to the size of the nonadiabatic region in the semi-cusp. Moreover, the transverse size of the ion flow in the axial region decreases with an increase in the magnetic field in the device. The total ion flow obtained by integrating the presented profiles is $I_i \approx 140$ A; a 135 A current goes to the annular plasma collector, and a 5 A current flows out through the aperture of the semi-cusp coil. The ion energy spectrum was measured by a grid analyzer located at the annular plasma collector. Figure 20 shows the measured delay curve, which is well approximated by the exponent $\exp(-eU/E_i)$; the average energy of ions leaving is $E_i \approx 320$ eV. The total power carried by the ions leaving is estimated to be $W_i = I_i E_i \approx 45$ kW.

The magnetic measurements show that the longitudinal current flows out through the annular slot of the semi-cusp near the separatrix and hits the grounded screen of the plasma collector. The average electron energy near the plasma collector, which is determined from the probe characteristics of the end detectors, is $E_e \approx 60$ eV. The total electron flux leaving the semi-cusp is $I_e = I + I_i$, where $I \approx 1$ kA is the longitudinal current, whereas the power carried away by electrons is estimated to be $W_e = I_e E_e \approx 70$ kW.

The radial energy losses are determined by measuring the heating of two diaphragms located in the input mirror of the MD at a 1-cm distance from each other. The power loss at the diaphragm located on the transport region side is found to be 3 kW, whereas the power loss at the diaphragm on the mirror-device side does not exceed 1 kW.

MHD Stability of Plasma

Plasma produced in the end cell is macroscopically stable. Measurements made with the help of sets of azimuthal probes and multichannel measurements of the H_α line emission indicate that there is no global plasma shift either during the plasma source operation or at the decay stage. In the plasma decay stage, oscillations of the ion current density with 10% amplitude and 5 kHz frequency are detected by both the individual detectors of the semi-cusp plasma collector and the peripheral Langmuir probes in the MD. To clarify the role of the semi-cusp, we performed an experiment in which the semi-cusp was switched off. The plasma remained globally stable, and the time dependences of the diamagnetic signals in the MD did not change. In the decay stage, the relative amplitude of the density oscillations at the plasma periphery doubled. The motion of the plasma center in the decay stage was determined from the time dependences of the ion saturation currents to four peripheral probes equally spaced in the azimuthal direction. The plasma density profile was approximated by a Gaussian profile. The position of the plasma column center was determined by minimizing the functional

$$W\{I_0, x_0, y_0, R_0\} = \sum_k (I\{x_k, y_k, I_0, x_0, y_0, R_0\} - I_k)^2,$$

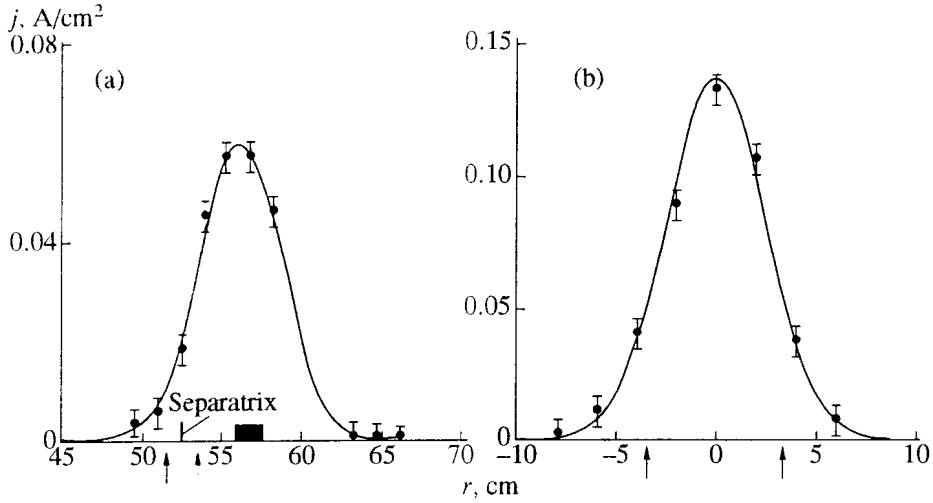

Fig. 19. Measured profiles of the plasma flows (a) to the annular plasma collector of the semi-cusp and (b) through the axial mirror. Arrows mark the boundaries of the adiabaticity region. The position of the separatrix is marked by the line segment, and the projection of the gas-discharge channel is shown by the rectangle.

where I_0 is the saturation current density at the plasma column axis; x_0 and y_0 are the transverse coordinates of the column axis with respect to the device; R_0 is the characteristic plasma density; x_k, y_k, and I_k are, respectively, the probe coordinates and saturation currents. Trajectories of motion of the center of the plasma column, for both regimes in which the semi-cusp was switched on and switched off, are shown in Fig. 21. With the semi-cusp switched off, the size of the region in which the plasma center moves is approximately twice as large as that for the case when the semi- cusp is switched on. In the course of experiments on fast hydrogen atom beam injection, in addition to experiments with two symmetrically located injectors, experiments were also performed with only one injector. No appreciable transverse shift of the initial plasma in the MD was observed, which is evidence for a substantial MHD stability of the end cell plasma with respect to the transverse displacement of the plasma column.

Gas Density in the Mirror Device

A set of pulse vacuum gauges was used to measure the pressure when the MD was being filled with a target plasma. Figure 22 shows the positions of the vacuum gauges and time dependences of the hydrogen pressure near the plasma. It is seen that, at 1.5 ms after the plasma source is switched on, the pressure starts to increase; the closer to the plasma jet, the greater is the increase in pressure. When hydrogen was fed to the plasma source, but the discharge was not ignited, the pressure in the MD started to increase 5 ms later. The similar effect of fast penetration of hydrogen into the MD was also observed in the Ambal-Yu; this effect is related to the formation of a jet of fast hydrogen atoms in the process of charge exchange of the jet protons with hydrogen atoms flowing from the source. [15].

Pulse Injection of Powerful Beams of Fast Neutrals into the Mirror Device

In order to study the properties of the initial plasma as a target plasma, we injected two pulse beams of fast hydrogen atoms into the MD. Two Start-2 injectors produced beams with 16 keV energy, 100 kA total equivalent current, and 200 ms duration [16]. Figure 23 shows that, during the injection, the diamagnetic signal from the loop placed outside of the shell increases. The linear growth of the diamagnetic signal during the injection and its subsequent decay with 1 ms characteristic time is evidence for the considerable confinement time of trapped fast ions. The growth of the diamagnetic signal

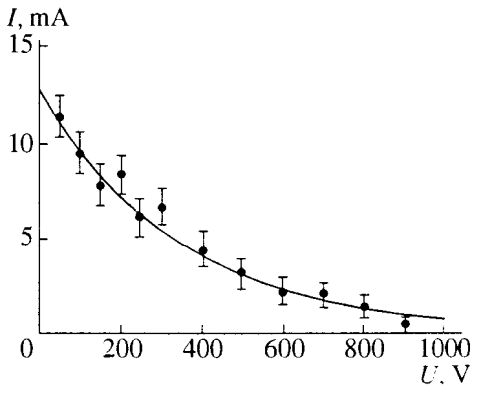

Fig. 20. Time delay of the ion current to the end electrostatic analyzer.

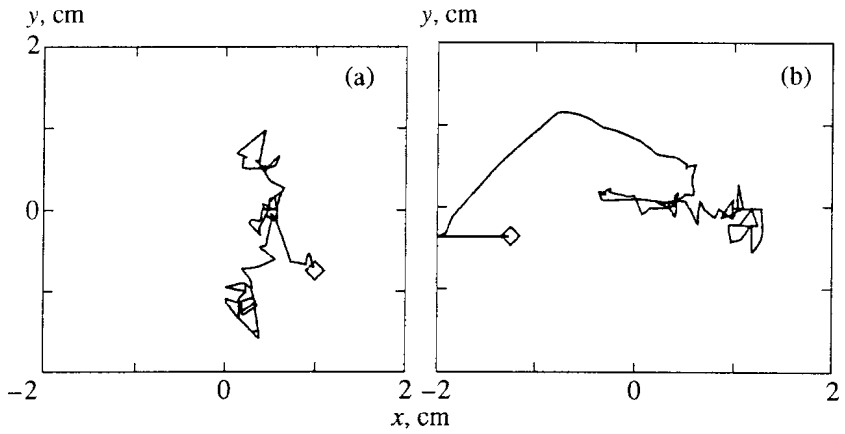

Fig. 21. Displacements of the center of the plasma column during the decay with the semi- cusp switched on (a) and switched off (b). Rhombuses mark the beginning of the motion.

is 0.3 of the maximum signal obtained from the target plasma. Because of the conducting shell installed at the center of the MD (magnetic field penetration time is 2 ms), the diamagnetic loop measures the signal from a small part of the plasma that extends behind the shell column (according to the model calculations, the length of this part is about 7 cm); therefore, the fast proton pressure is approximately equal to the target plasma pressure. It follows from the measured number of fast atoms (8%) trapped from injected beams that the average density of fast protons accumulated to the end of the pulse in the 20 l volume is $\sim 5 \times 10^{11}$ cm^{-3}.

DISCUSSION OF THE RESULTS

In order to produce hot initial plasma in the end cell, it is most important to suppress the electron heat exchange between the MD and the transport region. As it follows from the experimental data, the thermal insulation at the axis and at the plasma periphery is provided by the minimum of the plasma potential in the input mirror. The potential minimum results from the density minimum, which arises because of reflection of the anisotropically heated ions from increasing magnetic field in the input mirror. The existence of this potential minimum observed in the experiment agrees with the previously obtained results. However, in the intermediate region around the axis, close to the input mirror, the potential minimum is absent despite a decrease in the plasma density. In this region, the longitudinal electric field responsible for the considerable longitudinal electron current exists. An intense electron current through the input mirror strongly suppresses the thermal loss from the MD in the intermediate region around axis. For the 100 A/cm^2 current density and 2×10^{12} cm^{-3} plasma density, the flow-averaged electron velocity is 3×10^8 cm/c, which corresponds to 25 eV energy. The electron velocity in the flow is greater than the thermal velocity; as a result the thermal transport from the MD to the transport region is suppressed.

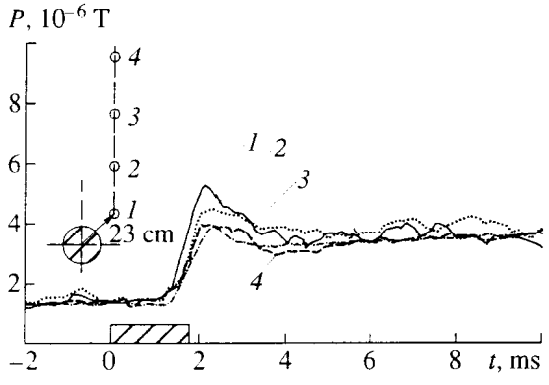

Fig. 22. Time dependence of the hydrogen pressure in the MD.

Another factor determining the production of the hot initial plasma is ion heating by the electrostatic oscillations arising as a result of the onset of Kelvin–Helmholtz instability. The cause of this instability (nonuniform radial profile of the transverse electric field) and its basic manifestation (driving of intense wide-spectrum oscillations of the azimuthal electric field) are close to those observed and studied previously in the MAL device [12]. An interesting feature of the instability evolution in the end cell in the case when the plasma jet has a length twice as large as in [12], is that the even modes with $m = 2, 4$ are dominated by the odd ones with $m = 1, 3, 5$ (Fig. 13), whose amplitude is an order of magnitude larger. As was mentioned above, a nonlinear competition of azimuthal modes occurs in the long plasma jet [12], which manifests itself as the energy transfer from the short-wavelength part of the fluctuation spectrum, where the Kelvin–Helmholtz instability is driven, to the long-wavelength part. As a result of the mode competition, the amplitude of the

first azimuthal harmonic turns out to be so large that its effect on the rest of the spectrum becomes substantial. In particular, it is possible that the odd harmonics dominate over even harmonics because of the strong first harmonic cause the nonlinear driving of only odd modes.

High-frequency oscillations of the plasma potential are related to the arc type of discharge in the plasma source. The discharge current breaks into current loops corresponding to different cathode spots existing for a finite time. When one of the spots disappears, the voltage drop in the other loops increases, and, since some of the current loops are terminated at the end cell plasma, the plasma potential changes. Thus, the plasma source generates a white noise, and, although the high-frequency oscillation power is low, its presence is substantial for stochastic heating, since it provides effective phase breaking.

Let us consider the plasma behavior in the MD. The increased plasma density in the center of the MD and considerable confinement time $\tau_{s\,exp} \sim 500$–700 μs obtained from the decay rate of the diamagnetic signal show that, in the MD, trapped ions appear, whose behavior is governed by the classical processes. For $n = 6 \times 10^{12}$ cm^{-3}, $T_i = 200$ eV and $T_e = 50$ eV, the classical ion scattering time and ion–electron energy transfer time are $\tau_i \approx 310$ μs and $\tau_{ie} \approx 1900$ μs, respectively. The ion confinement time in the MD with respect to their escape through the loss cone is [17] $\tau_{\parallel} = 0.525\tau_i(\ln R + \sqrt{\ln R}) \approx 420$ μs, and energy loss time due to the loss cone is $\tau_\varepsilon = 1.348\tau_i \ln R = 570$ μs. The ion energy loss time agrees well with the decay time of the diamagnetic signal. From the calculated value of the ion confinement time, which is confirmed by the probe measurements of the plasma density at the decay stage, we obtain that the ion flow from the MD with the plasma volume $V \sim 20$ l is equal to 40 A. In addition, the plasma density in the MD increases with a rate corresponding to the 10 A trapped ion current. Thus, ions are trapped from the flow propagating through the MD, and their flow corresponds to a 50 A current. The measurements made at the end plasma collector give the value $I_i \sim 140$ A. This means that, due to the ion reflection from the input mirror, only a small fraction of the 2 kA ion flow produced by the plasma source arrives at the MD.

Numerical simulation of the collisionless ion flow in front of the input mirror in the presence of a pronounced Kelvin–Helmholtz instability was performed by the Monte Carlo method. Calculations were performed for 10^5 particles, which begin to move at a 1 m distance from the input mirror; this distance corresponds to the ion mean free path. The velocity distribution function of ions moving toward the mirror was assumed to be half-Maxwellian with the initial temperature 50 eV. The motion of each particle in the magnetic field was broken into small steps along the axis; at each step, the magnetic momentum and total energy were assumed to be constant, and, at every transition to the next step, the ion transverse energy changed by a value determined by the heating rate. The plasma flow parameters are obtained by averaging over all particles, and, for the 5 eV/μs transverse energy growth rate [18], the following values were obtained at the input mirror: 1.5×10^{12} cm^{-3} plasma density, 175 eV ion temperature, and 175 A ion flow through the mirror. These calculated plasma parameters are sufficiently close to the experimentally measured ones.

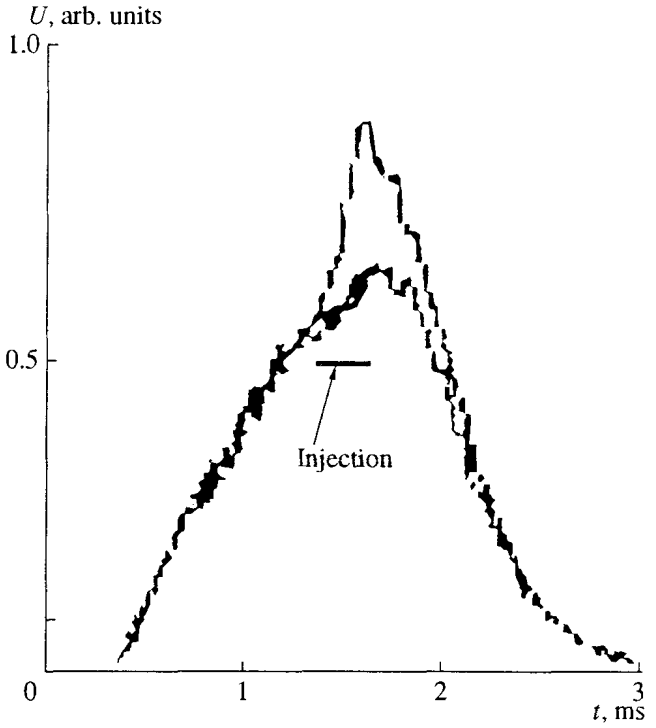

Fig. 23. Change in the diamagnetic signal in the MD during the injection of the beam of fast hydrogen atoms.

In the MD, the trapping of transit ions occurs as a result of an increase in the pitch angle due to both scattering and the growth of the transverse energy in the process of stochastic heating by the low-frequency oscillations. Temperature of protons (180 eV) entering the MD is measured by the probes at the input mirror and by the diamagnetic loops in front of it. In order to illustrate the proton trapping in the MD, we present the numerical estimates. For a proton with energy $E = 200$ eV and a pitch angle at the input mirror close to $\pi/2$, the transit time required to pass from the input mirror to the center of the MD is $\tau \approx 10$ μs; $n\tau$ is estimated to be 3.4×10^{13} cm^{-3} μs, which corresponds to $\tau_1 \approx 5.7$ μs for the density at the center of the MD. Consequently, the proton moving from the input mirror to the center of the device scatters by the angle $\delta\theta_1 \approx \sqrt{\tau_1/\tau_i} \approx 0.14$. The growth rate of the transverse proton energy in the device can be estimated from the fact that the

energy gained by trapped protons compensates the energy transferred to electrons and maintains the increase in ion temperature with time. It follows from Fig. 3 that $T_i/dt \approx 0.04$ eV/μs, and the rate of the growth of the transverse energy is $dE/dt = 3/2(T_i/\tau_{ie} + dT_i/dt) = 0.2$ eV/μs. When the proton moves to the center of the device, its transverse energy increases by $\delta E = \tau dE/dt = 2$ eV. Due to this increase in energy, protons with a pitch angle in the interval from θ_c to $\theta_c - \delta\theta_2$ (where $\theta_c = \arcsin 1/\sqrt{R} = \pi/6$ is the loss cone angle and $\delta\theta_2 \approx \delta E/E \approx 0.01$) are trapped in the MD. Since $\delta\theta_1 > \delta\theta_2$, the main process responsible for proton trapping is scattering; however, the increase in the transverse energy of protons also is important, because it provides the return of the trapped particles from the boundary of the loss cone into the confinement region and decreases the scattering into the loss cone. The fraction of the flow of transit ions with the pitch angles between θ_c and $\theta_c - \delta\theta_1$ with respect to the total flow of transit ions is $2\delta\theta_1/\theta_c$. Scattering occurs in two pitch angle directions; therefore, the flow of protons scattered in the direction of the confinement region and trapped in the MD is estimated to be equivalent to the current $I_1 \approx I_i\delta\theta/\theta_c \approx 40$ A. When the particle motion from the center of the MD to the output mirror is taken into account, the fraction of the trapped protons increases by approximately $\sqrt{2}$, and the final estimate for the trapped proton flow is $I_1 \approx 56$ A, which is close to the above-determined value of the flow of trapped protons.

Let us discuss the behavior of the electron component. In the MD, the electrons are confined in a potential well with depth $\Delta\varphi \sim 100$ V. Since the well depth is relatively small $\Delta\varphi \sim 2T_e/e$ and the ratio of ion to electron temperature is ~4, the classical loss of the trapped electrons exceeds the ion loss. In the MD with fast ion beam injection, the ion and electron losses are equal, but in order to have equal classical losses, it is necessary to have $\Delta\varphi \sim 5T_e/e$ for $E_i/T_e \sim 10$ [19]. According to the Pastukhov formula [17], the loss of the trapped electrons from the MD corresponds to a current of order $I_e \sim 300$ A, and the power carried away by electrons through the mirrors is $W \approx I_eT_e \sim 15$ kW. The trapping of electrons in the MD, which compensates for their loss, occurs due to scattering and deceleration of electrons carrying the longitudinal current. The difference between profiles of input and output currents (curves *3* and *4* of Fig. 10) is evidence for the electron trapping in the plasma. The radial profile of the trapped electron density is broadened due to diffusion. When trapped electrons escape through the output mirror, the resulting current profile broadens with respect to the profile of the flow of transit electrons because of the summation of currents. The profile of the current of electrons entering through the input mirror narrows due to subtraction of the flow of trapped electrons escaping the MD. As a result, the electron current at the output of the MD must be broader than the current at the input, which is confirmed by the profile measurements. The amount of electrons trapped in the MD corresponds to the classical processes. The specifics of the considered processes is that, due to the low plasma density in front of the input mirror, the electrons carrying the longitudinal current are accelerated by the electric field (collisions can be neglected in this case) and enter the MD with a considerable longitudinal energy of 100 eV and low temperature. The transit time of electrons through the MD is $\tau \sim 0.3$ μs, Coulomb scattering time of transit electrons by ions and electrons is $\tau_s \sim 1.5$ μs, and the energy loss time determined by collisions with electrons is $\tau_e \sim 3$ μs. Thus, electrons passing through the MD scatter by the angle $\delta\theta \sim \sqrt{\tau/\tau_s} \sim 0.4$, and suffer the energy spreading $\Delta E \sim E_e\sqrt{\tau T_e/\tau_e E_e} \sim 20$ eV and the energy loss $\delta E_e \sim E_e\tau/\tau_e \sim 10$ eV. A part of the electron flow is trapped in the MD due to the reflection from the output mirror and scattering, and the capture factor ~0.3 is quite natural. At the same time, the electron distribution function in the MD is of "flow" type (the dispersion in velocities is less than the directed velocity): this can cause the onset of instabilities resulting in additional scattering. The power carried away by electrons exceeds the power gained by electrons from the trapped ions, which is equal to $W_{ie} \sim 3/2nVT_i/\tau_{ie} \sim 3$ kW. The power gained by trapped electrons from the longitudinal electron current $I \sim 1$ kA flowing through the MD is $W_{ee} = I\delta E_e \sim 10$ kW. This electron heating is due to the current, but it is not Joule heating. Thus, the high electron temperature in the MD is maintained mainly by the energy transfer from the flowing electron current to electrons. The total electron heating power $W_e = W_{ie} + W_{ee} \approx 13$ kW agrees well with the above estimate for the power carried away by escaping electrons. As a whole, the classical behavior of the trapped electrons and ions, which was confirmed by the analysis performed, is important for successfully carrying out the planned experiments on powerful fast neutral beam injection and high-frequency heating.

The results of experiments on pulse injection of powerful beams of fast neutrals, which have shown the linear increase in the density of fast ions in the MD, are encouraging for futher experiments with the use of quasisteady powerful beams of fast ions. By using the beam injection with a total equivalent current of 100 A, we expect that fast ions with a density of 5×10^{12} cm^{-3} can be accumulated during the existence of the initial plasma: because this ion density is comparable with the initial plasma density, the further ion accumulation is possible. Some increase in the hydrogen density in the MD during the last stage of the existence of the initial plasma does not seem to be dangerous and can be suppressed by increasing the pumping rate and changing the regime of plasma source operation.

Discussion of interesting and important experimental data on the filling of the inner hollow region of the

longitudinal electron current inside the transport region and providing the MHD plasma stability in the MD, when the semi-cusp is switched off, is out of the scope of this paper and will be presented in further publications.

ACKNOWLEDGMENTS

This work was supported in part by the Ministry of Science and Technological Policy of the Russian Federation, State Program of Controlled Fusion and Plasma Processes; the International Science Foundation, grant no. RPE 000; and the Russian Foundation for Basic Research, project no. 95-02-05316 and 96-02-19296.

REFERENCES

1. Dimov, G.I., *Proc. Int. School of Plasma Phys.*, Varenna, 1987, p. 703.
2. Dimov, G.I., Davydenko, V.I., and Lysyansky, P.B., *Proc. 16th Eur. Conf. Controlled Fusion and Plasma Phys.*, Venice, 1989, vol. 13B, part II, p. 815.
3. Dimov, G.I., *Proc. 10th Int. School of Plasma Phys.*, Tbilisi, 1990, p. 157.
4. Dimov, G.I., *Proc. Int. Conf. on Open Plasma Systems for Fusion*, Novosibirsk, 1993, p. 23.
5. Glyavin, M.Yu., Nusinovich, G.S., Pankratova, T.B., *et al.*, *Vopr. At. Nauki Tekh., Ser. Nucl. Phys. Res.*, 1990, no. 4, p. 65.
6. Dimov, G.I., Ivanov, A.A., and Roslyakov, G.V., *Fiz. Plazmy*, 1982, vol. 8, p. 970 [*Sov. J. Plasma Phys.* (Engl. transl.), 1982, vol. 8, p. 546].
7. Gilev, E.A., Dimov, G.I., Kabantsev, A.A., *et al.*, *Pis'ma Zh. Eksp. Teor. Fiz.*, 1993, vol. 57, p. 621.
8. Akhmetov, T.D., Belkin, V.S., Bender, E.D., *et al.*, *Proc. 21st Eur. Conf. Controlled Fusion Plasma Phys.*, Montpellier, 1994, vol. 18B, part I, p. 446.
9. Belkin, V.S., Bender, E.D., Gilev, E.A., *et al.*, *Proc. Int. Conf. on Open Plasma Systems for Fusion*, Novosibirsk, 1993, p. 37.
10. Davydenko, V.I., Ivanov, A.A., Kabantsev, A.A., *et al.* *Diagnostika plazmy* (Plasma Diagnostics), Pergament, M.I., Ed., Moscow: Energoizdat, 1986, no. 5, p. 147.
11. Bender, E.D. and Chupriyanov, V.E., *5 Vsesoyuznoe soveshchanie po diagnostike vysokotemperaturnoi plazmy* (All-Union Conference on High-Temperature Plasma Diagnostics), Minsk, 1990, p. 230.
12. Kabantsev, A.A. and Taskaev, S.Yu., *Fiz. Plazmy*, 1990, vol. 16, p. 700 [*Sov. J. Plasma Phys.* (Engl. transl.), 1990, vol. 16, p. 406].
13. Liewer, P.C., *Nucl. Fusion*, 1985, vol. 25, p. 543.
14. Chirikov, B.V., *Voprosy teorii plazmy* (Reviews of Plasma Physics), Kadomtsev, B.B., Ed., Moscow: Energoatomizdat, 1984, no. 13, p. 3.
15. Gilev, E.A., Dimov, G.I., Kabantsev, A.A. *et al.*, *Proc. Int. Conf. on Open Plasma Systems for Fusion*, Novosibirsk, 1993, p. 485.
16. Davydenko, V.I., Roslyakov, G.V., and Savkin, V.Ya., *Vopr. At. Nauki Tekh., Ser:. Nucl. Phys. Res.*, 1983, no. 2, p. 67.
17. Pastukhov, V.P., *Voprosy teorii plazmy* (Reviews of Plasma Physics), Kadomtsev, B.B., Ed., Moscow: Energoatomizdat, 1984, no. 13, p. 160.
18. Kabantsev, A.A. and Taskaev, S.Yu., *Fiz. Plazmy*, 1992, vol. 18, p. 635 [*Sov. J. Plasma Phys.* (Engl. transl.), 1992, vol. 18, p. 331].
19. Dimov, G.I., Zakaidakov, V.V., and Kishinevskii, M.E., *Fiz. Plazmy*, 1976, vol. 2, p. 597 [*Sov. J. Plasma Phys.* (Engl. transl.), 1976, vol. 2, p. 326].

Translated by A. D. Smirnova